Sustainable Cities and Society 100 (2024) 105043

Contents lists available at ScienceDirect

Sustainable Cities and Society

journal homepage: www.elsevier.com/locate/scs

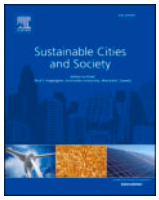

Assessing the spatiotemporal impact of users' exposure and vulnerability to flood risk in urban built environments

Gabriele Bernardini [a], Tiago Miguel Ferreira [b,*], Pilar Baquedano Julià [c], Rafael Ramírez Eudave [c], Enrico Quagliarini [a]

[a] DICEA Department, Università Politecnica delle Marche, Ancona, Italy
[b] College of Arts, Technology and Environment, School of Engineering, University of the West of England (UWE Bristol), Bristol, United Kingdom
[c] Institute for Sustainability and Innovation in Structural Engineering (ISISE), Department of Civil Engineering, University of Minho, Guimarães, Portugal

ARTICLE INFO

Keywords:
Flood safety
Urban built environment
Users' exposure
Users' vulnerability
Risk assessment

ABSTRACT

Flood risk in an urban built environment depends on the combination of the hazard, the vulnerability of the built environment itself and its infrastructure (referred to as physical vulnerability), and the exposure and vulnerability of the people residing, working or visiting it (i.e., their human condition). However, factors affecting those people vary over space and time depending on the uses of the built environment. This research offers a methodology for combined spatiotemporal flood risk assessment, providing hourly variations in risks due to hazard, physical vulnerability, users' exposure, and vulnerability. A mesoscale approach is adopted by collecting and managing data for each open space in the urban layout (e.g., street, square) and the facing buildings. In particular, users' exposure and vulnerability are investigated for indoor and outdoor uses and their temporalities, providing hourly distributions of users' density, age, familiarity with the built environment, and direct exposure to the floodwaters. Then, the Analytical Hierarchy process is used to combine risk factors. Finally, the application to a case study application (an urban district in Guimarães, Portugal) demonstrates how users' factors alter the risk over the day within the same mesoscale element and considers different elements which share the same hazard and physical vulnerability.

1. Introduction

Cities are widely affected by flood risk worldwide (Jha et al., 2012), especially when considering urban areas located in floodplains or riverines or exposed to coastal events or flash floods (Nixon, 2016; Bernardini et al., 2021; Young & Jorge Papini, 2020; da Silva et al., 2022; Kvočka et al., 2016). Given the complexity of the urban built environment, flood risk assessments should thoroughly evaluate the conditions of each urban component, by integrating contextual (geographical) data with mesoscale information (Bernardini et al., 2021; Sharifi, 2019). This mesoscale assessment pertains to the configuration of lots, urban blocks, and urban open spaces within the urban area, and it is a powerful assessment scale because it connects the features of micro-scale elements, such as buildings, including their specific characteristics and their spatial relationships with other surrounding buildings and open spaces as well as the street network components. This mesoscale level represents the minimum scale necessary for understanding interactions between users and amongst users and the built environment (Sharifi, 2019). In this sense, the mesoscale is also fundamental for risk assessment and for the analysis and development of strategies to enhance resilience (Bernardini et al., 2021; Sharifi, 2019).

The flood source should be investigated along with how floodwaters can spread within the urban layout and, therefore, consider the characteristics of streets, squares, other open spaces, and infrastructure, such as the sewer systems (Mignot et al., 2019; Fahy et al., 2019). Factors influencing floods include the plan layout, elevation, horizontal surface typology, drainage density, the connection between other built environment elements, and the characteristics of obstacles and other vertical elements, such as building façades acting as channel boundaries in compact urban fabrics (Bunmi Mudashiru et al., 2022; Mannucci et al., 2022; Mignot et al., 2020). The combination of these elements forms the foundation for the hazard and physical vulnerability assessment explored in this work (Ferreira & Santos, 2020; De León & Carlos, 2006), as detailed in Section 2.

* Corresponding author at: College of Arts, Technology and Environment, School of Engineering, University of the West of England (UWE Bristol), Frenchay Campus, Coldharbour Lane, Bristol BS16 1QY, United Kingdom.
E-mail address: Tiago.Ferreira@uwe.ac.uk (T.M. Ferreira).

https://doi.org/10.1016/j.scs.2023.105043
Received 31 July 2023; Received in revised form 28 September 2023; Accepted 5 November 2023
Available online 6 November 2023

Nevertheless, the urban built environment also hosts users whose presence in outdoor and indoor spaces of the city varies depending on spatiotemporal dynamics correlated to the intended use of the built environment (Storch & Downes, 2011; Wang et al., 2020; Quagliarini et al., 2023). Therefore, users' exposure and vulnerability play a fundamental role in quantifying urban flood risk. Their assessment should be performed at a fine-scale level (Hossain & Meng, 2020) though. In view of the urban dynamics and its correlation with the intended use of the built environment (Quagliarini et al., 2023; Hossain & Meng, 2020; De Angeli et al., 2022), one of the critical issues in exposure concerns the population distribution and the quantification of the number of people in the given flood-prone area (https://www.undrr.org/terminology/exposure, last access: 08/05/2023), since such a distribution can directly contribute to estimating possible casualties occurring in case of a flood emergency (Fan et al., 2018). Amongst the various components affecting users' vulnerability (De León & Carlos, 2006; Flanagan et al., 2011), those associated with the "human condition", are particularly relevant due to their spatiotemporal variations. This is because certain users' features, namely those related to age and gender (UNISDR, 2017), as well as direct exposure to the floodwaters and associated threats, may require specific safety responses during emergency conditions (e.g., sheltering in place, evacuation processes) (Bernardini et al., 2021; Haynes et al., 2009).

Although this reference context is well-consolidated, most of the existing risk assessment methods are affected by some recurring limitations. They are generally focused on territorial approaches (Bunmi Mudashiru et al., 2022; Hossain & Meng, 2020; da Silva et al., 2020; Chen, 2022; Aidinidou et al., 2023), i.e., the analysis at the *meso* (down to each building block or a single open space, e.g., a street) (Ferreira & Santos, 2020; Yin et al., 2016) and micro (i.e., single building) (Hossain & Meng, 2020; Wahba et al., 2022) scales have been limitedly investigated. In these cases, techniques often rely on a cell-based discretisation of the urban area (Caprario & Finotti, 2019; Han & Mozumder, 2022), which can be useful to overlap data with simulation results on floodwater spreading (Wahba et al., 2022) but do not account in a detailed and accurate way the specificities of the exposed elements.

Previous methods heavily rely on multi-criteria analysis techniques, which are well-established in the flood risk field (Musungu et al., 2012). Amongst them, the Analytical Hierarchy Process (AHP) (Saaty, 1980; Goepel, 2013) is one of the most-used methods. It can be easily coupled with Geographic Information Systems (GIS), ensuring not only the representation of data in correlation with the urban scenario features (da Silva et al., 2020; Chen, 2022; Aidinidou et al., 2023) but also rapid data collection and update of details in case of a variation in the urban built environment conditions. Some efforts have also been made to include social factors in risk assessment, such as human lives (Aidinidou et al., 2023). Similarly, approaches have been proposed to perform risk assessment and describe the impact of alternative risk mitigation strategies (Han & Mozumder, 2022; Piyumi et al., 2021). Nevertheless, efforts to include users' exposure and vulnerability in risk assessment are still needed, especially focusing on the mesoscale level, which can combine reliability and swiftness of application while considering the spatiotemporal variations of risks due to such dynamic factors.

Given the above context, this paper aims to define and apply a methodology for spatiotemporal flood risk assessment, combining hazard and physical vulnerability assessments with the analysis of the users' exposure and vulnerability. Data are collected and managed at a mesoscale level (Sharifi, 2019), which relates to the configuration of the urban open spaces (both streets and squares), as they are the essential elements in the flood network (Bernardini et al., 2021; Yin et al., 2016). Mesoscale data (i.e. related to each open space as a whole) and microscale data (concerning the facing buildings, their features and those of their users) are collected and are aggregated for risk assessment purposes by deriving risk factors and a final index representing the mesoscale level conditions.

In particular, hazard and physical vulnerability are assessed using "static" data, depending on an assumed peak flow scenario and the built environment features. Users' exposure and vulnerability are considered dynamic over time, and the developed method allows providing their hourly variations according to validated methodologies (Quagliarini et al., 2023). Users' density, age, familiarity with the built environment, and direct exposure to the floodwaters are considered essential factors for risk assessment (Bernardini et al., 2021; Mannucci et al., 2022; UNISDR, 2017; Haynes et al., 2009). Those are managed in this work using a GIS tool and combined to derive a final risk index using the AHP. An urban district in the historic urban centre of Guimarães, Portugal, is used as a case study for the method application and capability demonstration. This case study represents a critical scenario since historical urban built environments are affected by remarkable complexity levels in terms of position in risk-prone areas, narrow and intricate layout, building vulnerability, attraction of users (including visitors who are not familiar with the built environment and its risks) and low implementation of mitigation measures (Bernardini et al., 2021; Ferreira & Santos, 2020; Miranda & Ferreira, 2019).

2. Methods

The work is organised into four main phases, as shown in the workflow of Fig. 1. The first phase (detailed in Section 2.1) concerns the definition and combination of the physical vulnerability of the buildings and the level of flood hazard, which is achieved by adopting the methodology proposed by Ferreira and Santos (2020). At this point, data is organised into homogeneous conditions for each open space (or its composing parts) within the urban built environment, thus focusing on the pursued mesoscale approach orientated to the configuration of urban open spaces (Bernardini et al., 2021; Sharifi, 2019). Subsequently, methods and tools for the GIS-based management of such input data are defined (Section 2.2). The third phase (Section 2.3) concerns defining users' exposure and vulnerability assessment methods. This phase allows for defining the spatiotemporal variations of primary input data, such as the number of exposed users and their vulnerability in terms of age-related, position-related, and familiarity-based aspects. Finally, input data are organised into risk factors to support an Analytical Hierarchy Process (AHP)-based approach, which provides a space and time-dependant risk index (Section 2.4). The risk index is then used to compare risk scenarios in the case study.

As mentioned earlier, a part of the historic centre of Guimarães, Portugal, is used here to test the suitability of the workflow proposed in this investigation. With a population of approximately 157,000 residents, Guimarães is located in the District of Braga, in the northern part of the country. The city holds significant cultural and historical value as the "cradle" of Portugal, as it was the setting for the events that led to the independence of the Kingdom of Portugal in 1128. As can be seen in Fig. 2, the case study focuses on the historical zone of "Couros," named after a river that was historically used for the local leather treatment industry. It is still possible to observe several ancient granite basins and other remnants that reflect the preindustrial origins of this neighbourhood. Likewise, one can still find various old houses once part of the popular extramural settlements in the surrounding area.

The designation of Guimarães as the European Capital of Culture in 2012 led to a series of requalification works and interventions aimed at revitalising various urban areas, including Couros. As a result, this area has experienced a renewed sense of vitality, primarily attributed to the presence of a University of Minho campus, a youth hostel, and other cultural facilities. This context underscores the significance of assessing the exposure and vulnerability of its users to flood risk.

2.1. Physical vulnerability and hazard assessment and data collection

The urban built environment is initially divided into sub-areas, based on "links" and "nodes" representation orientated towards the street and open spaces networks (Yin et al., 2016). Specifically, each "link"

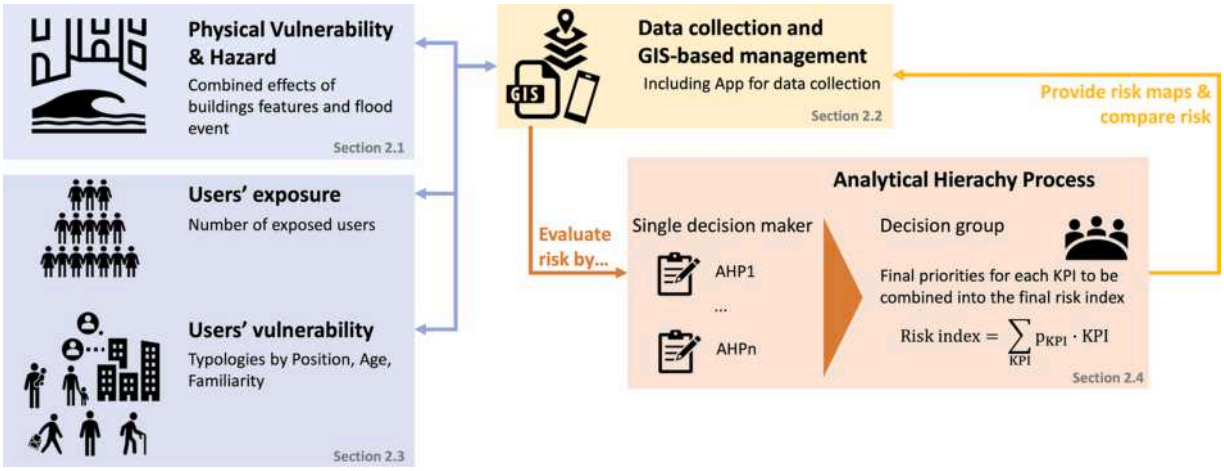

Fig. 1. Research workflow, pointing out the related methodological sections for each work phase.

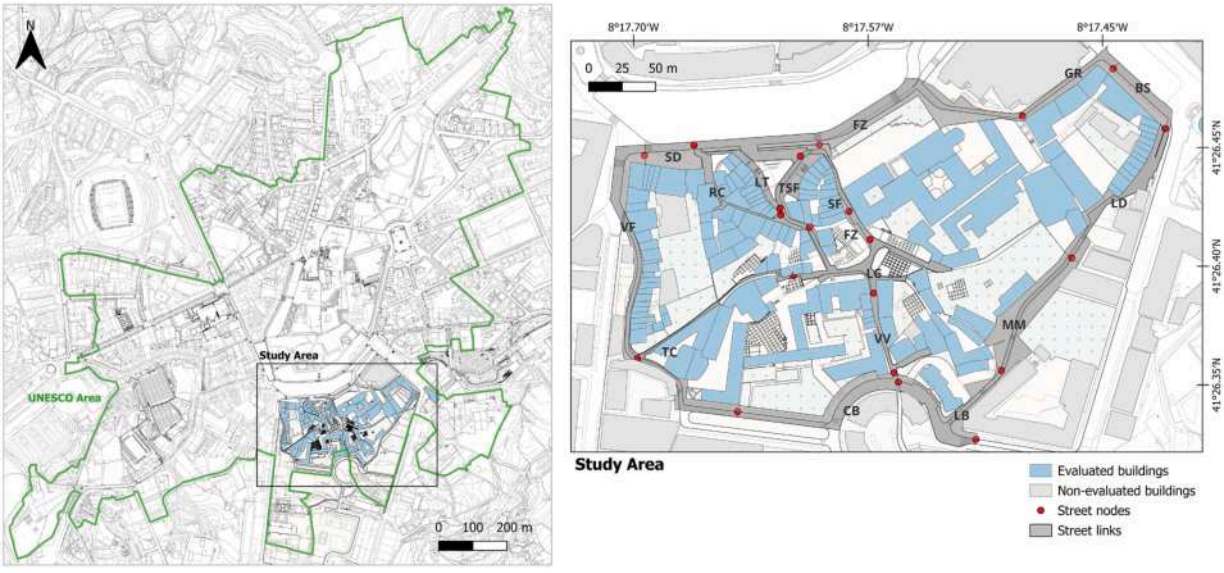

Fig. 2. Identification of the study area within the Historic Centre of Guimarães and codification of the nodes (red dots) and links (grey areas) adopted in this analysis.

represents a street or a square, delimited by two crossroads, considered as "nodes" in the network. "Nodes" represent potential decision points for users in a flood emergency, while each "link" also defines a well-defined "open channel" for floodwaters (Bernardini et al., 2021). The resulting division is illustrated in Fig. 2, which also displays the location of the study area within the Historic Centre of Guimarães.

The flood risk assessment methodology proposed by Ferreira and Santos (2020) was applied in this investigation to evaluate the hazard and physical vulnerability of buildings to flooding. Specifically, flood hazard assessment employed the hydrologic-hydraulic method, which provided outputs related to flood extent, water depth, and velocity. The assessment process involved acquiring and preparing geometric data, estimating the peak flow, conducting hydraulic modelling, and performing GIS post-processing and mapping. Peak flow data was estimated for the 100-year flood by averaging results from four different methods in two sections. The first section, defined at the upstream inlet (35.95 m^3/s), corresponds to a contributing basin of 3.75 km^2. The second section was estimated at the downstream outlet of the modelled reach (54.15 m^3/s), with the difference (18.2 m^3/s) proportionally distributed across 11 pour points evenly spaced along the reach's length (1786 m); refer to Table 1 for details.

Pre-processing of geometric data was performed using the RAS Mapping tool in HEC-RAS 5.0.7 software. For specific details regarding the modelling process and results exportation process, please refer to Ferreira and Santos (2020).

The physical vulnerability of the buildings was evaluated using an index-based methodology, which, due to its simplified (but not simplistic) nature, has the great advantage of being able to be used in the

Table 1
Flow data used in the hydraulic model (Ferreira & Santos, 2020).

POUR POINT	Upstream inlet	A	B	C	D	E	F	G	H	I	J	K
Reach Length [m]	0.00	33.0	51.6	158.9	260.0	651.2	782.7	1013.7	1146.4	1252.6	1344.2	1495.1
Affluent Q_P [m^3/s]	35.95	0.45	1.53	0.60	2.00	1.16	0.32	1.97	7.55	0.38	0.97	1.27
Sum Q_P [m^3/s]	35.95	36.40	37.93	38.53	40.53	41.69	42.01	43.98	51.53	51.91	52.88	54.15

context of macro-scale evaluations, where more detailed methodologies cannot be used while maintaining an excellent balance between the volume of input data required and the accuracy of the results (Romão et al., 2016; Baquedano Julià & Ferreira, 2021). As detailed in Miranda and Ferreira (2019), the methodology adopted in this research assesses the physical vulnerability of the buildings through two vulnerability components – an exposure and a sensitivity component –, which, when combined, allow us to quantify the physical vulnerability of the buildings to flood inundation. The exposure component consists of a single parameter, wall orientation, which assesses how the building's orientation may influence its physical vulnerability. This assessment takes into account the characteristics of the main façade wall, including the number and size of its openings, as well as its relative positioning concerning the direction of floodwater flow. The sensitivity component focuses on the physical characteristics of the building and evaluates its material characteristics, condition (or conservation state), number of stories, age, and heritage status. It is worth noting that these indicators were defined by Miranda and Ferreira (2019) based on a comprehensive review of analogous indicators proposed for assessing similar building typologies and structural characteristics under compatible conditions, refer to Mebarki et al. (2012), Schwarz and Maiwald (2008), Stephenson and D'Ayala (2014), Ferreira et al. (2014); Santos et al. (2013), Maio et al. (2017).

2.2. Data collection and GIS-based management

A digital checklist was developed in QGIS software (QGIS Development Team. QGIS, 2017) to systematically record information on-site regarding the current state and use of buildings. The Mergin cloud storage service (https://merginmaps.com) and its corresponding QGIS plugin, both freeware, were used for this purpose. Additionally, the Input app, freely available and compatible with mobile devises such as smartphones, facilitated the workflow based on the online distribution of the database, enabling real-time editing and data collection in the field.

The data collection strategy implemented ensured the capture of a wide range of information, including details about building conditions, occupancy status, access points, outdoor areas, and current uses. Specifically, a series of on-site surveys were conducted to identify abandoned or uninhabited buildings, delineate public spaces, sidewalks, and open but inaccessible areas, and associate each building with its primary access point and corresponding outdoor area. This phase was critical as it provided precise information about building accessibility. In some cases, buildings appeared to have multiple access points on maps, but surveys revealed that they were only accessible from a single entrance.

Furthermore, on-site surveys also confirmed the current uses of the buildings, which included not only the type of use (refer to Appendix A for details) but also insights into the operating and opening hours of public and service buildings. In cases where this information could not be obtained on-site, it was sourced from publicly available data, such as Google Maps (as seen in other literature, e.g., De León & Carlos, 2006), or through telephonic contact. It is important to note that while this work didn't implement this, some commercial establishments and public buildings provide data on their websites regarding footfall within specific time intervals.

A total of 143 buildings, with seven different uses, were surveyed and considered in the analysis presented herein – refer to Fig. A1 in the Appendix A. These data were then used to support the users' exposure and vulnerability parameters (Section 2.3) and assess the risk factors (Section 2.4).

2.3. Users' exposure and vulnerability assessment

Users' exposure and vulnerability, and their temporalities, are assessed according to previous quick methodologies orientated to the analysis of each mesoscale element as itself (Quagliarini et al., 2023). The method relies on GIS data about the geometry (i.e., gross surface, covered area, number of floors) and the intended use of indoor and outdoor areas. These data are firstly combined with occupant loads [pp/m^2] and use-related temporalities (with a one-hour approximation of timetables) to derive users' exposure over time. Table 2 summarises the occupant load depending on the main rules for temporalities, which refer to the areas opened or closed to the public. Then, the users' typologies for each area are derived depending on (1) the position of the users within the built environment by distinguishing indoor users (i.e., residents and non-residents) and outdoor users (i.e., only outdoor users, that are passers-by, and prevalent outdoor users, such as people attending bar and restaurant dehors), as shown in Table 2; (2) the familiarity with the built environment, its urban layout, and its hazards, by conservatively considering that only residents are classified as fully familiar; (3) the age of the users, which is also related to autonomy in motion, distinguishing between toddlers (0 to 4 years), parent-assisted children (5 to 14 years), young users (15 to 19 years), adults (20 to 69 years) and elderly (70+ years). Each of these classifications about users' typologies provides additional temporalities in built environment use. In particular, data on users' age are collected according to statistics at the municipal level, while the following temporalities have been considered: toddlers and elderly are always present at home; parents-assisted children and young users are not considered at home from 8 to 13 because they are at school; adults are not considered at home from 8 to 18, since they are at workplaces/universities, except from unemployed adults (for the case study, 10 % of the population) who are always at home. Finally, the vulnerability of users is also assessed in terms of their

Table 2
Intended use of indoor and outdoor areas in the built environment: related occupant load, general temporalities, and typologies of users. NA: not associable to the given condition.

Intended Use	Occupant Load [pp/m^2] when open to public	when close to public	General Temporalities for "open to public" occupant load application	Main typology of users
INDOOR AREAS				
residential	0.05	NA	0–24	Residents
office, including institutional buildings	0.4	0.1	depending on the opening times	Non-residents
school	0.7	0.1	depending on the opening times	Non-residents
hospital	0.1	0.1	0–24	Non-residents
commercial	0.7	0.1	depending on the opening times	Non-residents
religious	0.7	0	depending on time for religious services	Non-residents
museum	0.7	0.1	depending on the opening times	non-residents
theatre	1.2	0.1	depending on the opening times	non-residents
hotel	0.4	NA	0–24	Non-residents
bar and restaurants	0.7	0.1	depending on the opening times	Non-residents
sport	0.4	0.1	depending on the opening times	Non-residents
OUTDOOR AREAS				
dehors	0.4	0	depending on the opening times	prevalent outdoor users
massgathering areas	2	NA	depending on the event	prevalent outdoor users
pedestrian area	0.1	0	7–24	only outdoor users
carriageways and parking areas	0	0	0–24	NA

vertical position in the built environment, calculating the number of users on the ground floor of each building.

The demographic characterisation of the users relied on the 2012 Census data obtained from the National Institute of Statistics (Statistics Portugal). The data, fully available in an open-access database, includes information for the civil parishes of Oliveira, São Paio, and São Sebastião, which encompasses the study area. Specifically for the context of this research, this database was used to get key demographics of the population, including gender, age (in 10-year intervals from 0 to 100 or more), and the percentage of foreign residents.

2.4. Risk factors and AHP consensus group

"The collected data have been organised to extract the risk factors and establish the hierarchical structure illustrated in Fig. 3. This structure was developed based on prior research (De León & Carlos, 2006). Fig. 3 also provides an overview of the alternatives and the calculation methods associated with each criterion/risk factor, as determined through the application of the Analytical Hierarchy Process (AHP), which was utilised to integrate these factors and generate the final risk indicator, denoted as R (Saaty, 1980; Goepel, 2013).

The physical vulnerability (from Section 2.1 data) is combined with the hazard according to previous works (Ferreira & Santos, 2020), thus obtaining a unique combined risk factor on Physical Vulnerability and Hazard *PVH* [-] described by three risk levels (low, middle, and high). In this way, factors relating to flood and the Built Environment are described as a whole to show the combined effects of the hazard in the specific scenario. Three uniform descriptive category levels are also associated with the numerical range (0 to 1): 0≤low risk<0.33, 0.33≤moderate risk<0.67, and 0.67≤high risk≤1.

The exposure *E* [-] (from Section 2.3 data) is calculated as the ratio between users' density of the assessed mesoscale element and the maximum acceptable users' density, herein considered equal to 4pp/m^2. In particular, the users' density has been calculated in respect of the gross indoor area plus the outdoor area (that is, the area of the street/square facing each building). E is capped by 1.0 if the density exceeds the maximum acceptable density.

Three risk factors are finally defined to describe the users' vulnerability (from Section 2.3 data), namely:

(1) The quantity of flood-exposed users in respect of the population in the area *UVp* [-].*UVp* is then calculated by summing up the number of users outdoors and on the ground floor of each building in the area and dividing this sum by the total number of exposed users. In this way, the factor considers direct flood effects on users who should evacuate or move upstairs in case of a flood event (Mignot et al., 2019).

(2) The ratio *UVa* [-] between the number of users who can be classified as age-vulnerable (i.e., toddlers, parent-assisted children, elderly) and the total number of exposed users, so to consider individual vulnerability in reaction and movement (Bosina & Weidmann, 2017; Lee et al., 2019; Cox & Shand, 2010).

(3) The ratio *UVf* [-] between the number of users who are regarded as limitedly familiar or unfamiliar with the built environment, its urban layout, and its hazards (i.e., non-residents, only outdoor and prevalent outdoor users) and the total number of exposed users (Bernardini et al., 2019).

When all the users are associated with the specific vulnerability conditions, the users' vulnerability factors are considered continuous between 0 and 1, thus underlining maximum vulnerability scenarios for the given area.

In this work application, *PVH, E, UVa, UVp, UVf* and *R* are assessed univocally for each area of the scenario, and, according to their definitions provided above, *E, UVa, UVp, UVf* and thus *R* vary over time, while *PVH* is described as a unique value (thus regardless of the day time). As mentioned above, each of these risk factors is numerically defined to vary between 0 and 1, making them comparable for the whole risk assessment task. This choice ensures that *PVH, E, UVa, UVp, UVf* and *R* can be also comparable in different scenarios since maximum and minimum risk factors conditions are unique and well defined. As a consequence, the time-dependant and space-dependant assessment of the case study can be fully performed because the risk factors vary in the same range. Similarly, the methodology could allow the comparison of risk outcomes for different typical day conditions (e.g., working days versus holidays) and different urban areas.

The AHP Excel system (Goepel, 2018) (https://bpmsg.com/new-ahp-excel-template-with-multiple-inputs/) was used to derive the weight values for each factor thanks to a pair-wise comparison between them, using a linear integer scale ranging from 1 (same importance) to 9 (maximum importance of the considered risk factor in respect to the others). Basic calculation details according to the adopted approach and tool (Goepel, 2018) are shown in Appendix B, while the Excel files are available from the authors upon reasonable request. Priorities are calculated using the row geometric mean method (RGMM) (Goepel, 2013), considering that the sum of these priorities in the metrics is equal to one for each assessed single risk. The researchers of this work first compiled their own AHP by independently verifying that the specific Consistency Ratio CR was lower than 10 %.

Then, the data were aggregated in a consensus group by deriving the comparison matrix on the aggregation of individual judgments and using the same RGMM as the selected prioritisation method (Goepel, 2013; Dong et al., 2010). The methodology proposed in Goepel (2013), Goepel (2018) has been used to evaluate the inconsistencies and the AHP consensus indicator S* (i.e. to additionally verify its percentage value). S* is a homogeneity index based on the Shannon entropy (Goepel, 2013). When S* is close to 0 %, there is no consensus between the decision makers, while when S* is close to 100 %, the decision makers' results fully agree. Thus, higher S* values would imply a higher consensus of the single decision-makers involved in the AHP assessment.

Thanks to the adoption of a single comparison layer, the final metric

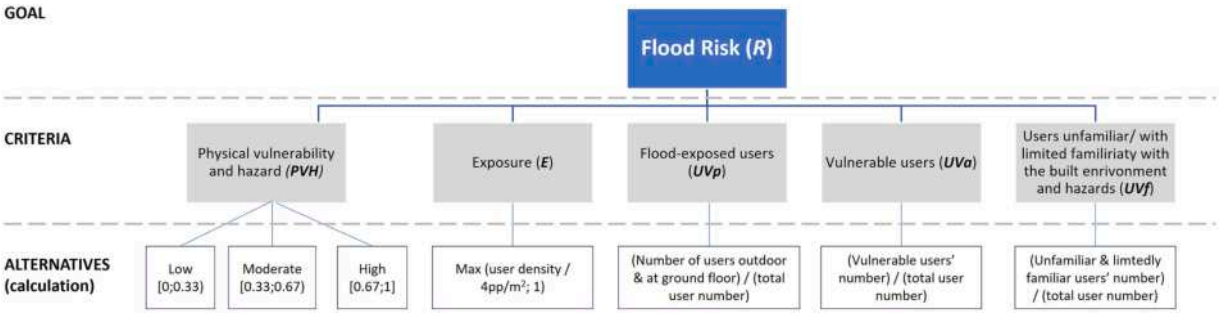

Fig. 3. Hierarchical structure of the flood risk assessment handled with AHP as described in the text.

output for a given risk will be equal to the sum of the multiplication between each risk factor aggregation-based priority and the related risk factor value (Saaty, 1980; Goepel, 2013; Dong et al., 2010), as shown by Eq. (1).

$$R = w_{PVH} \times PVH + w_E \times E + w_{UVp} \times UVp + w_{UVa} \times UVa + w_{UVf} \times UVf \quad (1)$$

Fig. 4 shows, on the left (Fig. 4-A), the summary of the final comparison matrix, which has been calculated according to the consensus group process, and, on the right (Fig. 4-B), the AHP results in terms of final weights for Eq. (1) and related uncertainties (vertical bars).

In general terms, all the decision makers' AHP and the aggregation are characterised by CR<10 %, confirming the acceptability of the pairwise comparisons. CR=2.6 %<10 % for the aggregated priorities, and, in addition, the Geometric Consistency Index GCI=0.096<0.37 as the threshold for CR=10 % with more than 4 criteria (Aguarón & Moreno-Jiménez, 2003). The S*=87.8 % confirms the good consensus between each decision maker, even though the dimension of the sample can impact the final S* result, as well as the different background skills of the individual decision-makers involved in the task. Finally, GIS-based maps representing each risk factor and the overall risk *R* are offered, using the same three uniform alternative levels associated with *PVH* to make them consistent according to homogeneous classification rules. These ranges hence are 0≤low values<0.33, 0.33≤moderate values<0.67, and 0.67≤high values≤1, pursuing the research approach on which the PVH assessment is based and making the final results consistent with it (Ferreira & Santos, 2020).

3. Results and discussion

To maintain the manuscript's compactness, the physical vulnerability results of the buildings are presented in Fig. A2, which can be found in the Appendix A. As mentioned earlier, these results are considered "static" as they depend on building features that are assumed to remain constant over the time frame considered in this study. These data were then combined with the hazard information to generate the Physical Vulnerability to Hazards (*PVH*) maps, also depicted in Fig. A2 in the Appendix A. *PVH* data is associated with each link in the road network and, consequently, each open space within the built environment.

In Fig. 5, the four user-related risk factors discussed in Section 2 are plotted using a boxplot representation to trace the main data distribution issues, including exposure (*E*) and the three factors related to users' vulnerability (*UVp, UVa,* and *UVf,*). Thus, for each risk factor, the boxplot distribution of data considers the sample of values for all the case study open spaces (thus, for the "links") and traces their minimum and maximum values (whiskers in Fig. 5) and the first, second and third quartile values (boxes in Fig. 5).

Notably, unlike the physical vulnerability of the buildings, users' exposure and associated vulnerability exhibit temporal variations according to their assessment methods. The analysis of the four plots provided in Fig. 5 reveals that schedules and urban dynamics play a significant role in shaping the levels of exposure and vulnerability. Consequently, the day was divided into five representative time spans, as highlighted in Fig. 5, thanks to their similar risk factors trends: night-time (from 0:00 to 7:00), early morning (up to 10:00), noon (up to 14:00), afternoon (up to 21:00), and evening (up to 24:00). These periods align with general guidelines for calculating and aggregating users' exposure and vulnerability based on intended uses and related spatiotemporal dynamics (Quagliarini et al., 2023).

In the following, the maps related to *E, UVp, UVa*, and *UVf* are respectively shown in Fig. 6, Fig. 7, Fig. 8, and Fig. 9, classified based on the ranges selected in Section 2.4 (0≤low values<0.33; 0.33≤moderate values<0.67; 0.67≤high values≤1). The results are presented in different panels (A-evening, B-early morning, C-noon, D-afternoon, and E-evening) organised according to the time spans defined in Fig. 5.

Most links are characterised by a predominant residential use (approximately 34 % of indoor gross surfaces), resulting in a homogeneous density of users over space and time. Dehors and mass gathering areas are limited to certain links in the case study (i.e., RM and LD), while most open spaces consist of pedestrian areas and roadways. Consequently, *E* values are generally low (see Fig. 6), given that residential use is associated with lower density levels (as discussed in Section 2.2). An exception is observed for a link with commercial use (upper right corner in Fig. 6 panels), which increases *E* conditions to moderate values from 10:00 to 21:00 during the opening hours of public activities.

Significant variations over time can be observed in the *UVp* maps in Fig. 7. Night-time (Fig. 7-A) is associated with less critical conditions, as expected, since the contribution of pedestrians in open spaces is considered close to zero. During night-time, links with moderate *UVp* are mainly characterised by taller buildings, as the reduction in the number of floors increases this indicator based on the criterion followed in this analysis. Data are poorly scattered, as shown by the boxplot in Fig. 5.

Conditions during noon (Fig. 7-C) and afternoon (Fig. 7-D) appear to be quite similar, reflecting an overall intermediate level of users' vulnerability, primarily due to an increase in outdoor users. Early morning (Fig. 7-B) and evening (Fig. 7-E) time spans exhibit the most critical *UVp* levels, as expected, owing to ground-floor uses open to the

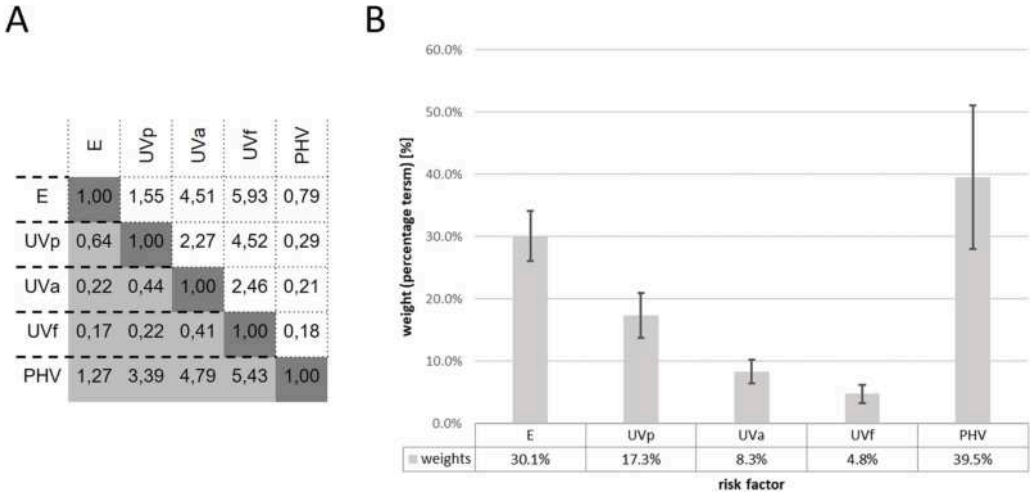

Fig. 4. Results of the AHP process and the consensus group tasks: A- summary of the final comparison matrix; B- risk factors and related weights, associated with vertical bars, that show the weights uncertainties.

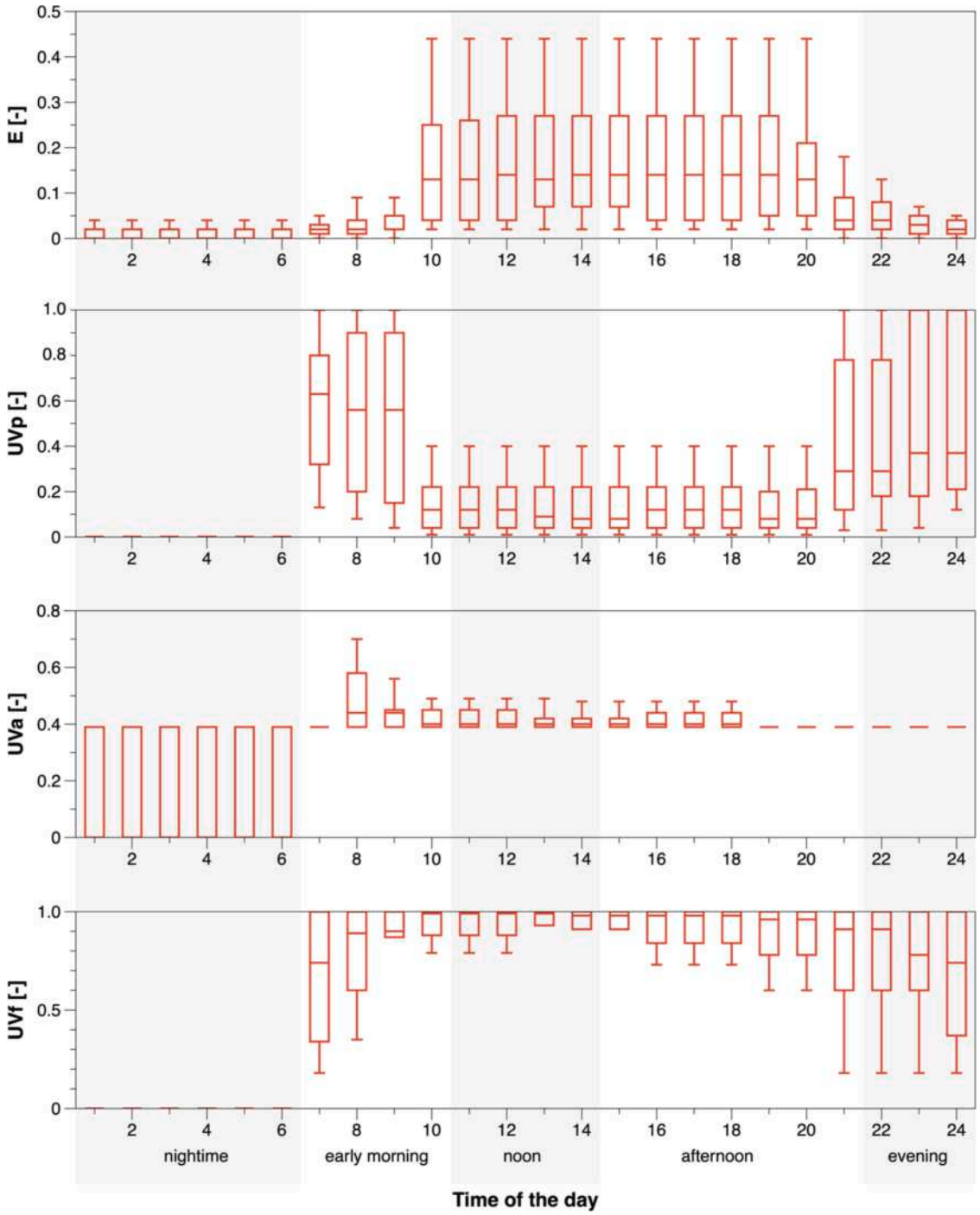

Fig. 5. Boxplot with the distribution of the E, UVp, Uva, and UVf results throughout the day.

public (e.g., schools as in MM or TC, single-floor institutional buildings, like in FZ, commercial activities, as in GR). Moreover, from a general perspective, *UVp* increases further during the evening due to a combination of these conditions with higher user density in residential buildings (adding users on the ground floors). Nevertheless, *UVp* values are not entirely homogeneous, as shown by the boxplot dispersion in Fig. 5 for the evening time.

Similar to *E* maps, *UVa* trends over time (Fig. 8) are primarily influenced by the sources of user distribution discussed in Section 2.2, particularly the use of a unified census database and the prevalence of residential intended use within the case study area. Consequently, *UVa* remains relatively consistent across the entire area over time. This result is also noticed by the boxplot trends in Fig. 5, which shows a quite constant median value and a generally low data dispersion. However, links hosting buildings open to the public (e.g., institutional buildings and commercial uses) exhibit more noticeable differences between night-time (Fig. 8-A) and evening (Fig. 8-E) compared to daytime, reflecting their respective opening hours.

As anticipated, *UVf* maps demonstrate significant differences between night-time (Fig. 9-A), when users are predominantly at home, and other time spans when values increase due to the combination of (a) non-familiar users' presence in public buildings and pedestrian areas and (b) a decrease in the number of residents, as per the adopted methodology (Quagliarini et al., 2023). Consequently, most links from early morning to evening exhibit moderate or high *UVf*. Conversely, during night-time, higher *UVf* values occur for links where

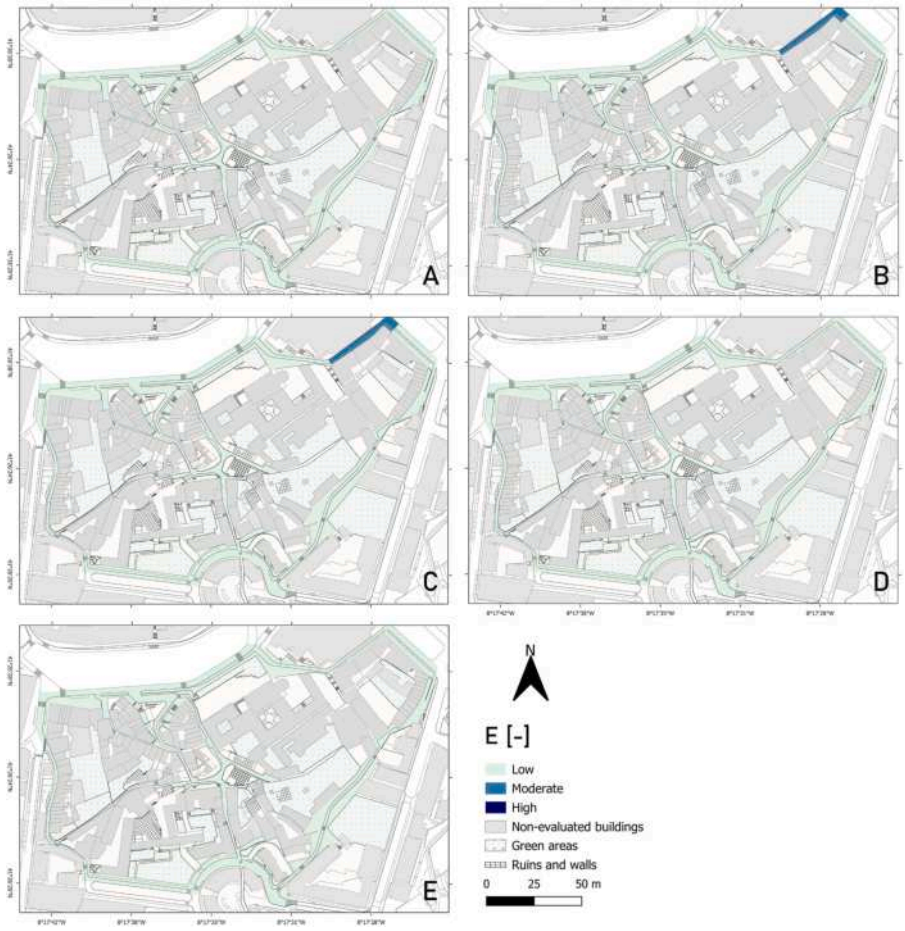

Fig. 6. *E* map over time: A-evening, B-early morning, C-noon; D-afternoon; E-evening.

accommodations (e.g., hotels) represent a significant percentage of the total gross surface area (e.g., TSF, with over 20 %). *UVf* also shows the highest values with respect to the other risk factors, as also graphically resumed by the boxplot in Fig. 5, which are quite concentrated towards the upper absolute risk values.

The overall *R* maps (in Fig. 10) appear to delineate a time-related hierarchy of conditions based on *E, UVp, UVa,* and *UVf* values. As anticipated, night-time conditions (Fig. 10-A) exhibit the lowest risk levels, with only a few links affected by moderate *R* values. In contrast, the afternoon (Fig. 10-D) and evening (Fig. 10-E) time spans display widespread moderate *R* values, reflecting the increasing impact of users' exposure and vulnerability. Early morning (Fig. 10-B) and noon (Fig. 10-C) conditions generally fall within the moderate *R* range, except for those links initially characterised by the lowest *PVH* values, indicating lower users' exposure and vulnerability. These findings confirm that the impact of users' exposure and vulnerability can influence the final floor risk level for each link. However, in the case study analysed herein, none of the links reaches high R range values since the *PHV* is typically balanced by users' exposure and vulnerability factors.

4. Conclusions and remarks

This work proposes a time-depending model for flood risk assessment based on a mesoscale assessment approach, focusing on the open spaces composing the urban built environment, their facing buildings and infrastructures, and their hosted users. This rapid assessment approach uses the Analytical Hierarchy Process (AHP) to merge and balance the different factors affecting flood risk over space and daytime. The historic centre of Guimarães, Portugal, was used as a pilot case study to show the main capabilities of the approach proposed in this investigation.

As discussed in this paper, including users' exposure and vulnerability significantly alters the overall risk compared to considering only the basic static conditions related to physical vulnerability and hazard (included in the *PVH* factor). While *PHV* remains constant over time and depends only on the urban open space and the flood characterisation, users' exposure *E* and vulnerability, which depends on the familiarity with the built environment *UVf*, vary considerably based on the buildings' uses and schedule time, assuming maximum values during the daytime, particularly in the noon and afternoon when public buildings are open and frequented by more users.

The users' vulnerability (*UVp*) based on their flood-prone position also varies due to similar factors, but it decreases during daytime hours. This is because, although more users are present, most are located on the upper floors of the buildings, which positively impacts their vulnerability to flooding. Conversely, age-dependant vulnerability (*UVa*) remains relatively stable over time due to the simplified but robust methodology used for data collection, relying on the Census database (De León & Carlos, 2006). Additional on-site surveys could be conducted in the future to enhance the accuracy of the assessment.

Time-dependant maps enable rapid identification of the riskiest areas, which vary over time but are generally concentrated where most public buildings are situated, thus aligning with the trends mentioned above. These maps focus on mesoscale elements, such as streets and squares, which represent integral links in the entire urban fabric. The expeditious methods employed for risk factor assessment ensure quick application and visualisation, making it feasible for stakeholders like public administration and their technicians, even those with limited expertise, to employ the method in wider urban areas.

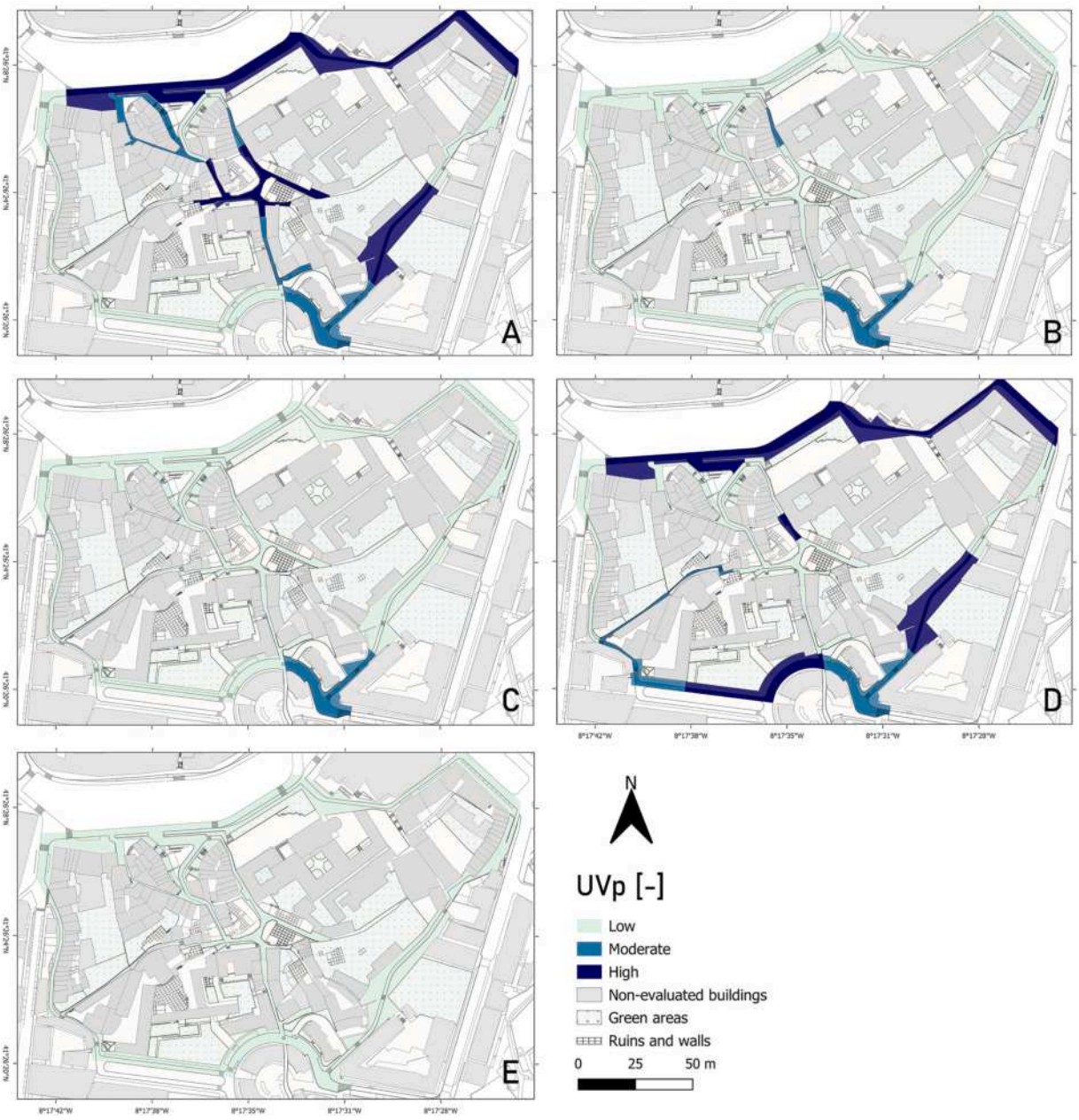

Fig. 7. UVp map over time: A: evening, B-early morning, C-noon; D-afternoon; E-evening.

Nonetheless, further improvements can be made by introducing additional levels of detail at a fine scale (e.g., individual buildings). This targeted approach could focus on structures with higher risk factor variability over time or those with the highest overall risk values. Moreover, future work steps could explore specific conditions of the built environment, particularly areas prone to mass gatherings, as they can exacerbate exposure by increasing the number of users and modifying users' demographics. In this sense, the authors are aware that the assessed users' exposure and vulnerability issues can be limited, although they are easy to retrieve and arrange in the whole risk assessment process. Furthermore, the adopted risk factors are directly correlated to the direct effects of floodwaters and possible evacuation scenarios on the built environment and its users. Future research can adopt the same AHP approach by including other dimensions of vulnerability (De León & Carlos, 2006; Flanagan et al., 2011), such as those relating to functional issues (thus increasing the analysis on general and floodwater-related infrastructures, as well as on other life-lines), economic and insurance-related factors, disability, vehicle availability affecting possible by-car evacuation, other social aspects such as community participation and preparedness/risk perception, administrative and environmental aspects. In this case, a multi-layer AHP could be used instead of a single layer (as adopted by this work), by enlarging and adapting the hierarchical structure proposed by the proposed methodology, but the same approach to risk factors should be pursued, making them comparable within the same 0 to 1 range.

The same methodology proposed in this work can also be effectively applied to retrofitted scenarios where the *PVH* factor can be altered through interventions on existing buildings, such as re-pointing or repairing the external render of the walls, adding resistance measures (e.g., flood skirts or barriers), and protecting potential water entry points, including vents, air bricks, and non-flood resilient doors and windows. This paves the way for a comprehensive flood risk management approach encompassing existing and future urban developments. By adopting the AHP-based model proposed in the paper and implementing

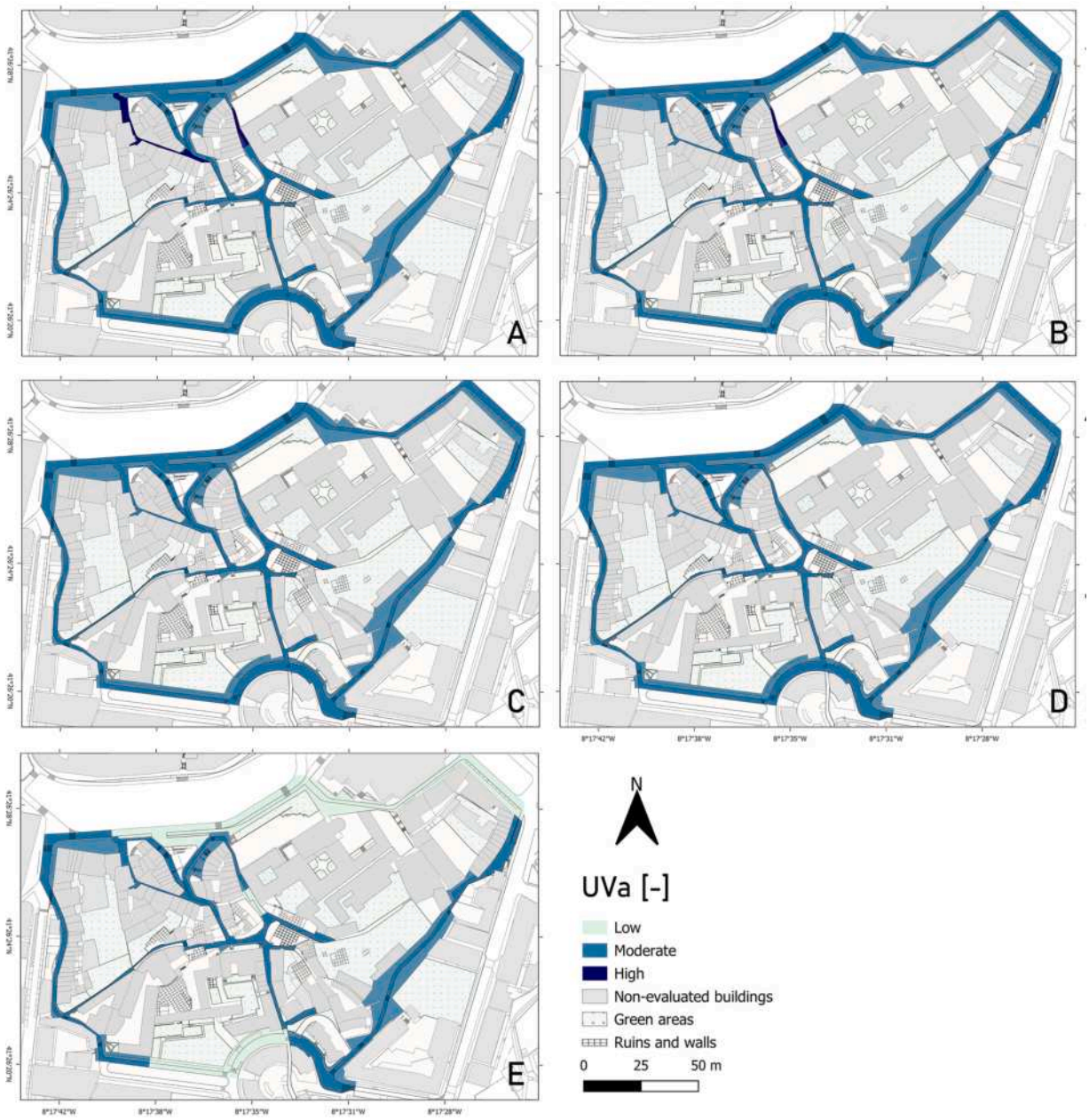

Fig. 8. UVa map over time: A: evening, B-early morning, C-noon; D-afternoon; E-evening.

flood vulnerability reduction strategies, stakeholders can pave the way toward more resilient and prepared urban landscapes.

Data availability statement

Data and the files used to derive the weight values for each factor will be made available upon request.

Declaration of Competing Interest

The authors declare that they have no known competing financial interests or personal relationships that could have appeared to influence the work reported in this paper.

Data availability

Data will be made available on request.

Appendix A

Fig. A1 includes a map identifying the buildings considered in the analysis presented in this paper, categorising the different types of building uses. For buildings with multiple uses, the type of use recorded at the ground floor level was the one identified in Fig. A1.

Fig. A2 includes a map displaying the distribution of the physical vulnerability results across the study area.

Finally, Fig. A3 includes a map illustrating the distribution of the obtained *PVH* results.

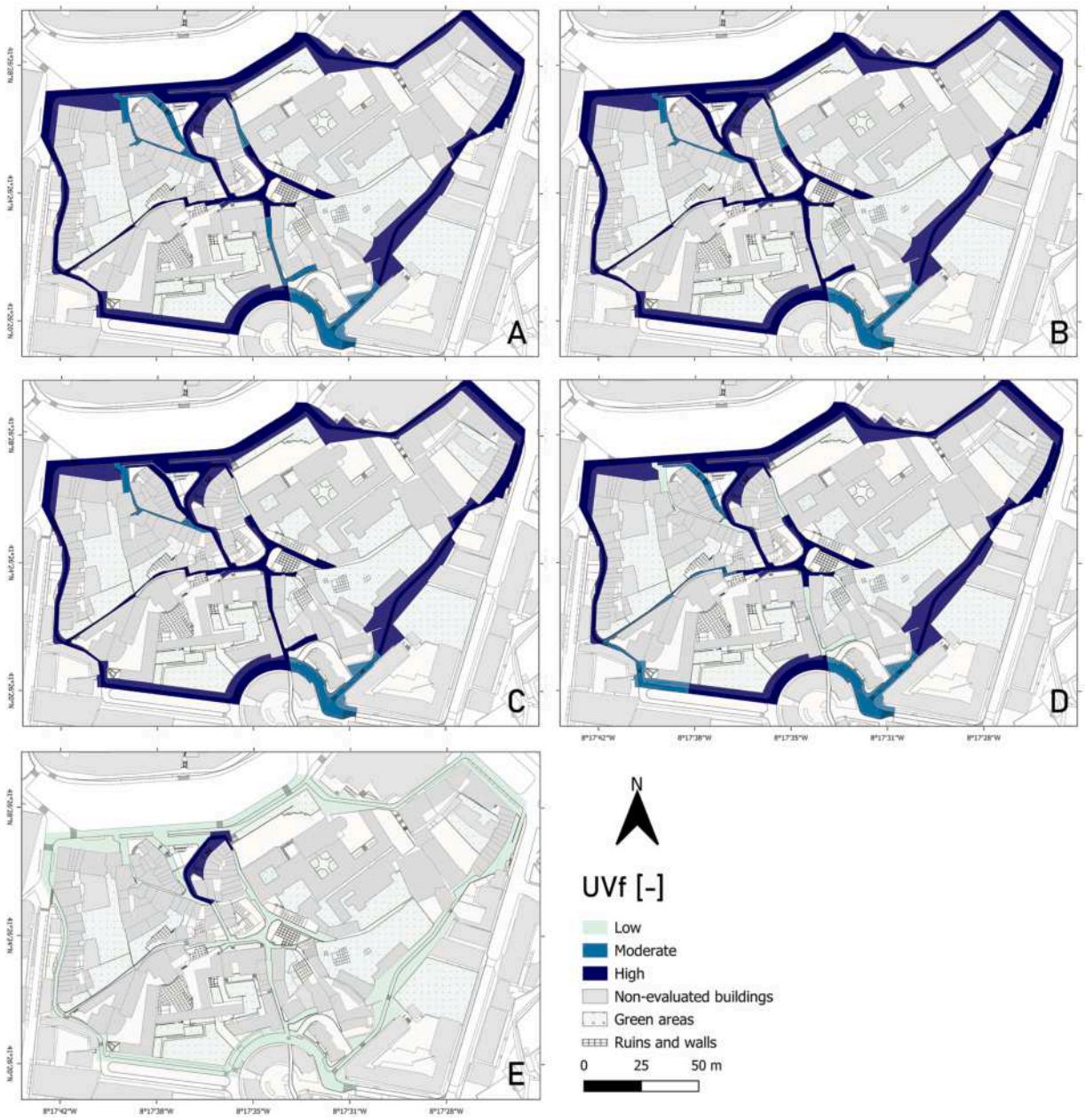

Fig. 9. UVf map over time: A: evening, B-early morning, C-noon; D-afternoon; E-evening.

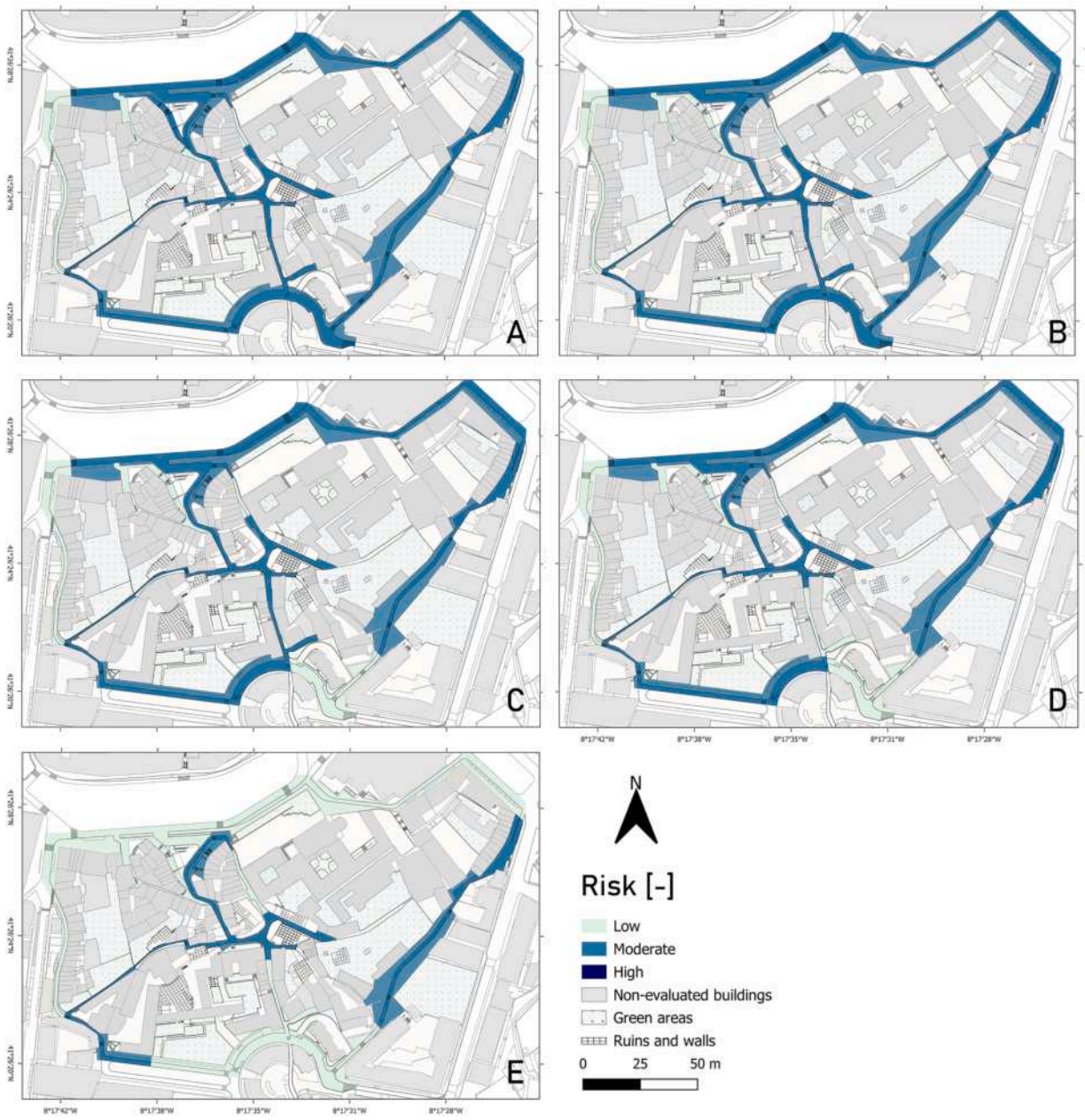

Fig. 10. R map over time: A: evening, B-early morning, C-noon; D-afternoon; E-evening.

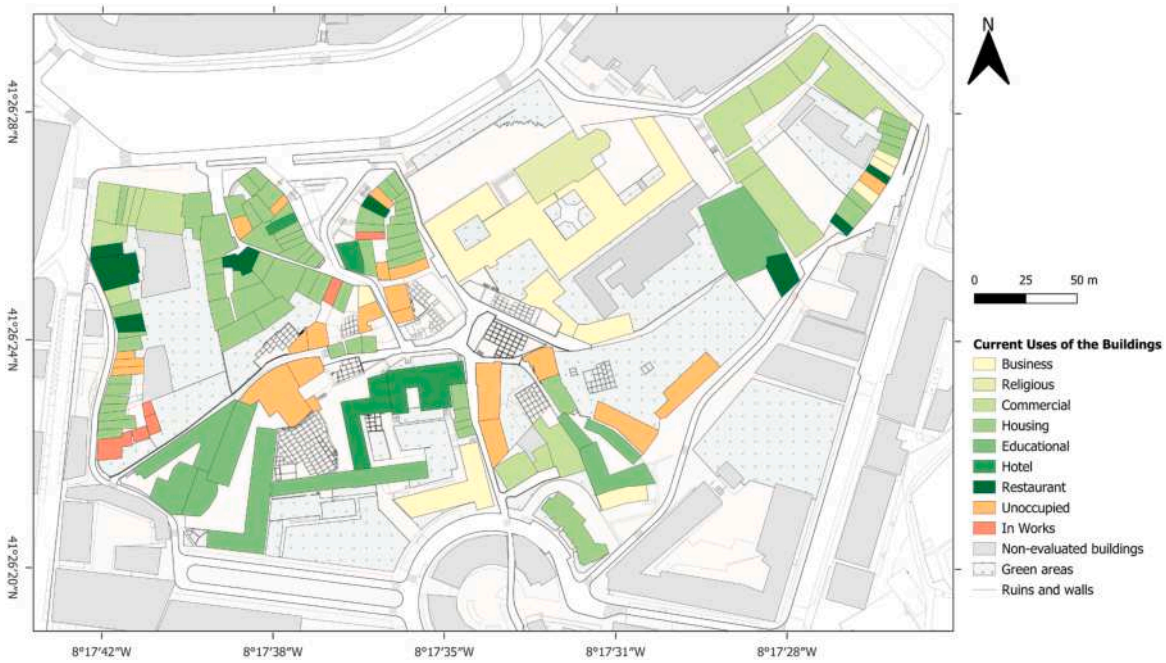

Fig. A1. Mapping of the buildings included in the analysis, highlighting their respective current uses.

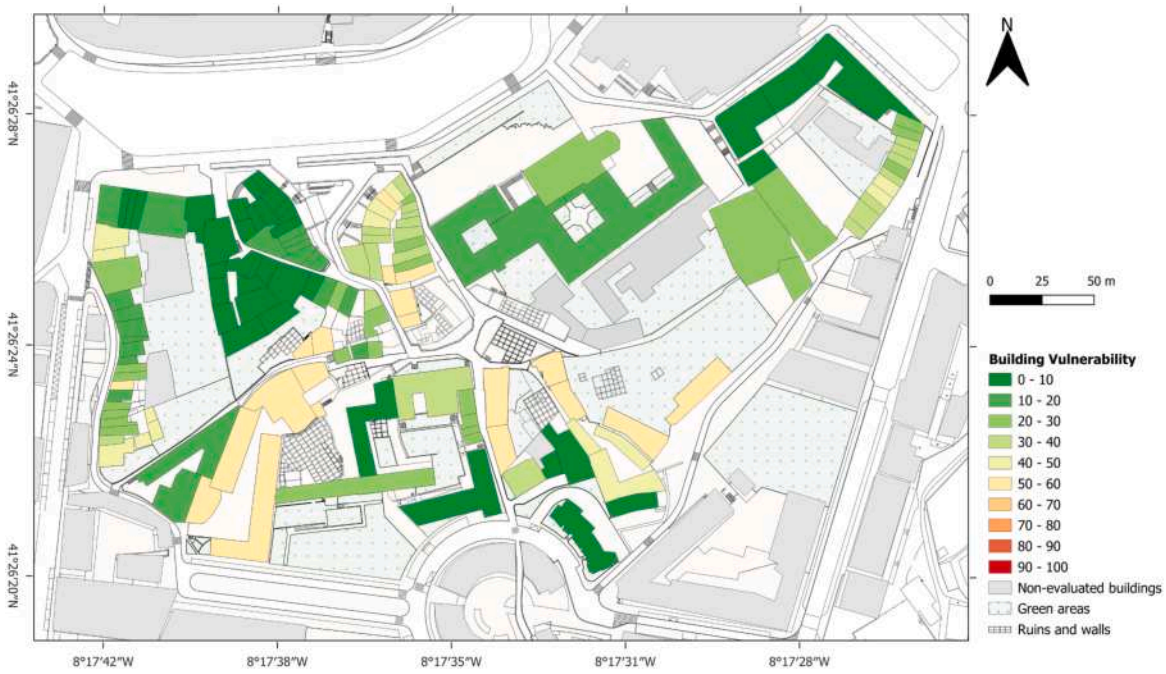

Fig. A2. Mapping of the physical vulnerability results obtained.

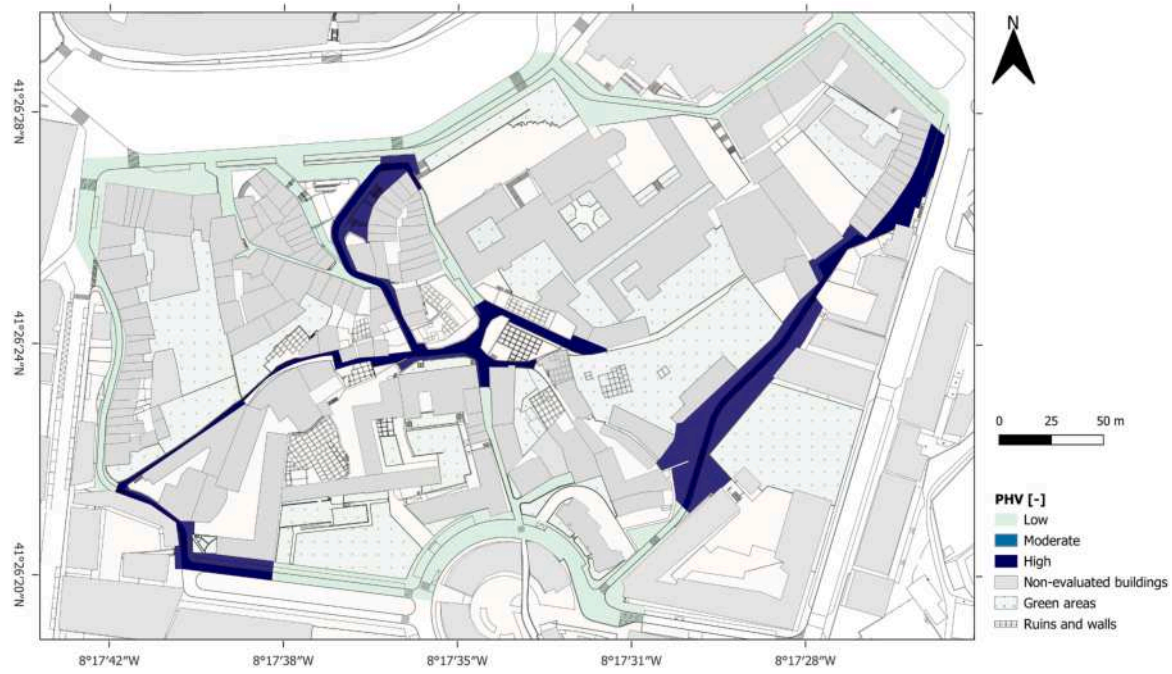

Fig. A3. Mapping of the PVH results obtained.

Appendix B

The verification of the proposed AHP-based assessment relies on the methods described by Goepel (Schwarz & Maiwald, 2008), using the related Excel software tool available at https://bpmsg.com/new-ahp-excel-template-with-multiple-inputs/. In particular, the following indicators have been calculated to evaluate the process quality: (A) for outputs of each decision maker (involved researcher) and of the whole group, the Consistency Ratio CR; (B) for the whole group outputs, the Geometric Consistency Index GCI and the Shannon index S*. The main procedures for calculation are shown in the following for the sake of brevity and completeness. Thus, for a more exhaustive overview of calculation methods, please refer to (Schwarz & Maiwald, 2008), while some additional references are included in the method description.

Given n the number of criteria (risk factors), we considered the pairwise comparison matrix $(n \times n)=(a_{ij})$, where $a_{ij}>0$, $a_{ij}a_{ji}=1$, and the cardinal transitivity in judgements ($a_{ij}a_{jk}=a_{ik}$ $\forall i,j,k$). Each a_{ij} is the judgement on the ratio between the compared priorities w_i/w_j.

CR is calculated according to the approach by Alonso and Lamata (Santos et al., 2013), as shown by Eq. (B1), and thus depends on n and the maximum eigenvalue of the pairwise comparison matrix λ.

$$CR = (\lambda - n)/(2.7699n - 4.3513 - n) \tag{B1}$$

GCI (Ferreira et al., 2014; Maio et al., 2017) is then assessed, as shown in Eq. (B2), as a function of the error e_{ij} obtained when the ratio ω_i/ω_j is approximated by a_{ij} ($e_{ij}=a_{ij}w_j/w_i$) and n. Approximated thresholds are used in this work to verify the GCI acceptability (i.e. for $n = 5>4$ and CR threshold=10 %, the GCI threshold is about 0.37).

$$GCI = \frac{2}{(n-1)(n-2)} \sum_{1 \le i < j \le n} log2\ e_{ij} \tag{B2}$$

Shannon index S* relies on the extension of the Shannon entropy H, which represents "a diversity index for the distribution of priorities amongst criteria" (Schwarz & Maiwald, 2008). The S* calculation considers the following main steps. The first step concerns the evaluation of standard alpha Shannon entropy $H\alpha$ for a group of K decision makers. As shown in Eq. (B3), $H\alpha$ equals the average Shannon entropy of all individual decision-makers (the researchers). Similarly, Eq. (B4) calculates the Shannon gamma diversity for the group aggregated priorities $H\gamma$. In both $H\alpha$ and $H\gamma$ calculation, the weights for the decision makers' impacts are equal ($I_1=I_2=\ldots=I_K=1/K$); thus, no priorities in the reliability of a decision maker's judgement are considered.

$$H\alpha = \left(- I_1 \sum_{i=1}^{n} w_{i1} \ln w_{i1} \right) + \left(- I_2 \sum_{i=1}^{n} w_{i2} \ln w_{i2} \right) + \ldots \tag{B3}$$

$$H\gamma = \sum_{i=1}^{K} (I_1 w_{i1} + I_2 w_{i2} + \ldots) \ln(I_1 w_{i1} + I_2 w_{i2} + \ldots) \tag{B4}$$

Then, true beta diversity of order one Dβ is calculated as in Eq. (B5), as function of $H\alpha$ and $H\gamma$. Dβ represents the "variations of priority distributions amongst decision makers within the group" (Schwarz & Maiwald, 2008) and thus varies from 1 (perfect agreement) to n.

$$D\beta = \frac{\exp H\gamma}{\exp H\alpha} \tag{B5}$$

The minimum alpha entropy $H\alpha,\min^*$ and maximum gamma entropy $H\gamma,\max^*$ for the considered n criteria and K decision makers can be calculated as in Eq. (B6) and Eq. (B7), respectively (Schwarz & Maiwald, 2008). In this work, the AHP comparison scale ranges from 1 to $M = 9$, while the criteria $n = 5$, thus the maximum priority is equal to $M/(n + M\text{-}1) = 0.6923$.

$$H\alpha, min^* = -\frac{M}{(n+M-1)}\ln\left(\frac{M}{n+M-1}\right) - \frac{n-1}{(n+M-1)}\ln\left(\frac{1}{n+M-1}\right) \tag{B6}$$

$$H\gamma, max^* = (n-K)\left[-\frac{1}{(n+M-1)}\ln\left(\frac{1}{n+M-1}\right)\right] - \frac{K+M-1}{n+M-1}\ln\left(\frac{1}{K}\frac{K+M-1}{n+M-1}\right) \tag{B7}$$

And finally, the S* indicator is calculated as in Eq. (B8) by applying $H\alpha,\min^*$ and $H\gamma,\max^*$ to the concept of equation B5. In view of the above, and according to the discussion on Dβ, S* ranges from 0 to 1 (or rather, expressed in percentage form, from 0 % to 100 %). The higher the value, the higher the consensus within the group.

$$S^* = \frac{(1/D\beta - D\alpha, min^*/D\gamma, min^*)}{(1 - D\alpha, min^*/D\gamma, min^*)} \tag{B8}$$

References

Aguarón, J., & Moreno-Jiménez, J. M. (2003). The geometric consistency index: Approximated thresholds. *European Journal of Operational Research, 147*(1), 137–145. https://linkinghub.elsevier.com/retrieve/pii/S0377221702002552.

Aidinidou, M. T., Kaparis, K., & Georgiou, A. C. (2023). Analysis, prioritization and strategic planning of flood mitigation projects based on sustainability dimensions and a spatial/value AHP-GIS system. *Expert Systems with Applications, 211*, Article 118566. https://doi.org/10.1016/j.eswa.2022.118566

Baquedano Julià, P., & Ferreira, T. M. (2021). From single- to multi-hazard vulnerability and risk in historic urban areas: A literature review. *Natural Hazard, 108*(1), 93–128. https://doi.org/10.1007/s11069-021-04734-5

Bernardini, G., Quagliarini, E., & D'Orazio, M. (2019). Investigating Exposure in Historical Scenarios: How People Behave in Fires, Earthquakes and Floods. In *Structural Analysis of Historical Constructions: An Interdisciplinary Approach* (pp. 1138–1151). Springer International Publishing.

Bernardini, G., Romano, G., Soldini, L., & Quagliarini, E. (2021). How urban layout and pedestrian evacuation behaviours can influence flood risk assessment in riverine historic built environments. *Sustainable Cities and Society, 70*, Article 102876. https://doi.org/10.1016/j.scs.2021.102876

Bosina, E., & Weidmann, U. (2017). Estimating pedestrian speed using aggregated literature data. *Physica A: Statistical Mechanics and its Applications, 468*, 1–29. https://doi.org/10.1016/j.physa.2016.09.044

Bunmi Mudashiru, R., Sabtu, N., Abdullah, R., Saleh, A., & Abustan, I. (2022). Optimality of flood influencing factors for flood hazard mapping: An evaluation of two multi-criteria decision-making methods. *Journal of Hydrology, 612*, Article 128055. https://doi.org/10.1016/j.jhydrol.2022.128055

Caprario, J., & Finotti, A. R. (2019). Socio-technological tool for mapping susceptibility to urban flooding. *Journal of Hydrology, 574*, 1152–1163. https://doi.org/10.1016/j.jhydrol.2019.05.005

Chen, Y. (2022). Flood hazard zone mapping incorporating geographic information system (GIS) and multi-criteria analysis (MCA) techniques. *Journal of Hydrology, 612*, Article 128268. https://doi.org/10.1016/j.jhydrol.2022.128268

Cox, R. J., & Shand, T. D. (2010). Australian Rainfall and Runoff revision project 10: appropriate safety criteria for people. *Water Research, 978*, Article 085825-9454.

da Silva, L. B. L., Alencar, M. H., & de Almeida, A. T. (2022). A novel spatiotemporal multi-attribute method for assessing flood risks in urban spaces under climate change and demographic scenarios. *Sustainable Cities and Society, 76*, Article 103501. https://doi.org/10.1016/j.scs.2021.103501

da Silva, L. B. L., Humberto, J. S., Alencar, M. H., Ferreira, R. J. P., & de Almeida, A. T. (2020). GIS-based multidimensional decision model for enhancing flood risk prioritization in urban areas. *International Journal of Disaster Risk Reduction, 48*, Article 101582. https://doi.org/10.1016/j.ijdrr.2020.101582

De Angeli, S., Malamud, B. D., Rossi, L., Taylor, F. E., Trasforini, E., & Rudari, R. (2022). A multi-hazard framework for spatial-temporal impact analysis. *International Journal of Disaster Risk Reduction, 73*, Article 102829. https://doi.org/10.1016/j.ijdrr.2022.102829

Fahy, B., Brenneman, E., Chang, H., & Shandas, V. (2019). Spatial analysis of urban flooding and extreme heat hazard potential in Portland, OR. *International Journal of Disaster Risk Reduction, 39*, Article 101117. https://doi.org/10.1016/j.ijdrr.2019.101117

Fan, Q., Tian, Z., & Wang, W. (2018). Study on risk assessment and early warning of flood-affected areas when a dam break occurs in a mountain river. *Water, 10*, 1369. https://doi.org/10.3390/w10101369

Ferreira, T. M., & Santos, P. P. (2020). An integrated approach for assessing flood risk in historic city centres. *Water, 12*, 1648. https://doi.org/10.3390/w12061648

Ferreira, T. M., Vicente, R., & Varum, H. (2014). Seismic vulnerability assessment of masonry facade walls: Development, application and validation of a new scoring method. *Structural Engineering and Mechanics, 50*, 541–561. https://doi.org/10.12989/sem.2014.50.4.541

Flanagan, B. E., Gregory, E. W., Hallisey, E. J., Heitgerd, J. L., & Lewis, B. (2011). A social vulnerability index for disaster management. *Journal of Homeland Security and Emergency Management, 8*(1), 3. https://doi.org/10.2202/1547-7355.1792. Article.

Goepel, K. D. (2018). Implementation of an online software tool for the analytic hierarchy process (AHP-OS). *International Journal of the Analytic Hierarchy Process, 10*. https://doi.org/10.13033/ijahp.v10i3.590

De León, V., & Carlos, J. (2006). *Vulnerability: A conceptual and methodological review*. Bonn, Germany: UNU-EHS: Studies of the University: Research, Counsel, Education. ISSN: 1816-1154, ISBN: 3981058240.

Dong, Y., Zhang, G., Hong, W. C., & Xu, Y. (2010). Consensus models for AHP group decision making under row geometric mean prioritization method. *Decision Support System, 49*, 281–289. https://doi.org/10.1016/j.dss.2010.03.003

Han, Y., & Mozumder, P. (2022). Risk-based flood adaptation assessment for large-scale buildings in coastal cities using cloud computing. *Sustainable Cities and Society, 76*, Article 103415. https://doi.org/10.1016/j.scs.2021.103415

Haynes, K., Coates, L., Liegh, R., Handmer, J., Whittaker, J., Gissing, A., & Opper, S. (2009). Shelter-in-place' vs. evacuation in flash floods. *Environmental Hazard, 8*, 291–303. https://doi.org/10.3763/ehaz.2009.0022

Hossain, M. K., & Meng, Q. (2020). A fine-scale spatial analytics of the assessment and mapping of buildings and population at different risk levels of urban flood. *Land use policy, 99*, Article 104829. https://doi.org/10.1016/j.landusepol.2020.104829

Jha, A. K., Bloch, R., & Lamond, J. (2012). *Cities and flooding*. The World Bank. https://doi.org/10.1596/978-0-8213-8866-2

Kvočka, D., Falconer, R. A., & Bray, M. (2016). Flood hazard assessment for extreme flood events. *Nat Hazards, 84*, 1569–1599. https://doi.org/10.1007/s11069-016-2501-z.

Lee, H. K., Hong, W. H., & Lee, Y. H. (2019). Experimental study on the influence of water depth on the evacuation speed of elderly people in flood conditions. *International Journal of Disaster Risk Reduction, 39*, Article 101198. https://doi.org/10.1016/j.ijdrr.2019.101198

Maio, R., Estêvão, J., Ferreira, T. M., & Vicente, R. (2017). The seismic performance of stone masonry buildings in Faial island and the relevance of implementing effective seismic strengthening policies. *Engineering Structures, 141*, 41–58. https://doi.org/10.1016/j.engstruct.2017.03.009

Mannucci, S., Rosso, F., D'Amico, A., Bernardini, G., & Morganti, M. (2022). Flood resilience and adaptation in the built environment: How far along are we? *Sustainability, 14*, 4096. https://doi.org/10.3390/su14074096

Mebarki, A., Valencia, N., Salagnac, J., & Barroca, B. (2012). Flood hazards and masonry constructions: A probabilistic framework for damage, risk and resilience at urban scale. *Natural Hazards and Earth System Sciences, 15*(5), 1799–1809. https://doi.org/10.5194/nhess-12-1799-2012

Mignot, E., Li, X., & Dewals, B. (2019). Experimental modelling of urban flooding: A review. *Journal of Hydrology, 568*, 334–342. https://doi.org/10.1016/j.jhydrol.2018.11.001

Mignot, E., Camusson, L., & Riviere, N. (2020). Measuring the flow intrusion towards building areas during urban floods: Impact of the obstacles located in the streets and on the facade. *Journal of Hydrology, 583*, Article 124607. https://doi.org/10.1016/j.jhydrol.2020.124607

Miranda, F. N., & Ferreira, T. M. (2019). A simplified approach for flood vulnerability assessment of historic sites. *Natural Hazard, 96*, 713–730. https://doi.org/10.1007/s11069-018-03565-1

Musungu, K., Motala, S., & Smit, J. (2012). Using multi-criteria evaluation and GIS for flood risk analysis in informal settlements of Cape town: The case of graveyard pond. *South African Journal of Geomatics, 1*, 77–91.

Nixon S. Horn J. Hödl-Kreuzbauer Edith Harmsel A. ter Van Erdeghem D. Dworak T. & European Commission Directorate-General for the Environment. (2016). *European overview assessment of member states' reports on preliminary flood risk assessment and identification of areas of potentially significant flood risk : final report*. Publications Office. doi:10.2779/576456.

Piyumi, M. M. M., Abenayake, C., Jayasinghe, A., & Wijegunarathna, E. (2021). Urban flood modeling application: assess the effectiveness of building regulation in coping with urban flooding under precipitation uncertainty. *Sustainable Cities and Society, 75*, Article 103294. https://doi.org/10.1016/j.scs.2021.103294

QGIS Development Team. QGIS. (2017). *Geographic Information System*. Open Source Geospatial Foundation. http://qgis.osgeo.org.

Quagliarini, E., Bernardini, G., Romano, G., & D'Orazio, M. (2023). Users' vulnerability and exposure in public open spaces (squares): A novel way for accounting them in multi-risk scenarios. *Cities, 133*, Article 104160. https://doi.org/10.1016/j.cities.2022.104160. London, England.

Romão, X., Paupério, E., & Pereira N, N. (2016). A framework for the simplified risk analysis of cultural heritage assets. *Journal of Cultural Heritage, 20*, 696–708. https://doi.org/10.1016/j.culher.2016.05.007

Saaty, T. L. (1980). *The analytic hierarchy process: Planning, priority setting & resource allocation*. MacGraw-Hill, New York Int. B. Co.

Santos, C., Ferreira, T. M., Vicente, R., & Mendes da Silva, J. A. R. (2013). Building typologies identification to support risk mitigation at the urban scale—Case study of the old city centre of Seixal, Portugal. *Journal of Cultural Heritage, 14*, 449–463. https://doi.org/10.1016/j.culher.2012.11.001

Schwarz, J., & Maiwald, H. (2008). Damage and loss prediction model based on the vulnerability of building types. In *Proceedings of the 4th international symposium on flood defence. Institute for catastrophic loss reduction*, 74-1–74-9.

Sharifi, A. (2019). Urban form resilience: A meso-scale analysis. *Cities, 93*, 238–252. https://doi.org/10.1016/j.cities.2019.05.010. London, England.

Stephenson, V., & D'Ayala, D. (2014). A new approach to flood vulnerability assessment for historic buildings in England. *Natural Hazards and Earth System Sciences, 14*(5), 1035–1048. https://doi.org/10.5194/nhess-14-1035-2014

Storch, H., & Downes, N. K. (2011). A scenario-based approach to assess Ho Chi Minh City's urban development strategies against the impact of climate change. *Cities, 28*, 517–526. https://doi.org/10.1016/J.CITIES.2011.07.002. London, England.

UNISDR. Flood hazard and risk assessment, Words into Action Guidelines: National Disaster Risk Assessment Hazard Specific Risk Assessment. United Nations Office for Disaster Risk Reduction. http://www.undrr.org/quick/11665.

Goepel, K. D. Implementing the analytic hierarchy process as a standard method for multi-criteria decision making in corporate enterprises – a new AHP excel template with multiple inputs, in: 2013. doi:10.13033/isahp.y2013.047.

Wahba, M., Mahmoud, H., Elsadek, W. M., Kanae, S., & Hassan, H. S. (2022). Alleviation approach for flash flood risk reduction in urban dwellings: A case study of fifth district, Egypt. *Urban Climate, 42*, Article 101130. https://doi.org/10.1016/j.uclim.2022.101130

Wang, B., Loo, B. P. Y., Zhen, F., & Xi, G. (2020). Urban resilience from the lens of social media data: Responses to urban flooding in Nanjing, China. *Cities, 106*, Article 102884. https://doi.org/10.1016/j.cities.2020.102884. London, England.

Yin, J., Yu, D., Yin, Z., Liu, M., & He, Q. (2016). Evaluating the impact and risk of pluvial flash flood on intra-urban road network: A case study in the city center of Shanghai, China. *Journal of Hydrology, 537*, 138–145. https://doi.org/10.1016/j.jhydrol.2016.03.037

Young, A. F., & Jorge Papini, J. A. (2020). How can scenarios on flood disaster risk support urban response? A case study in Campinas metropolitan area (São Paulo, Brazil). *Sustainable Cities and Society, 61*, Article 102253. https://doi.org/10.1016/j.scs.2020.102253